
Towards disentangling coupled electronic–vibrational dynamics in ultrafast non-adiabatic processes

V. Blanchet,[†] S. Lochbrunner,[‡] M. Schmitt, J. P. Shaffer, J. J. Larsen,[§] M. Z. Zgierski, T. Seideman and A. Stolow*

Steacie Institute for Molecular Sciences, National Research Council of Canada, 100 Sussex Drive, Ottawa, Ontario, Canada K1A 0R6

Received 10th February 2000

Published on the Web 6th April 2000

Femtosecond time-resolved photoelectron spectroscopy is emerging as a new technique for investigating polyatomic excited state dynamics. Due to the sensitivity of photoelectron spectroscopy to both electronic configurations and vibrational dynamics, it is well suited to the study of non-adiabatic processes such as internal conversion, which often occur on sub-picosecond time scales. We discuss the technical requirements for such experiments, including lasers systems, energy- and angle-resolved photoelectron spectrometers and new detectors for coincidence experiments. We present a few examples of these methods applied to problems in diatomic wavepacket dynamics and ultrafast non-adiabatic processes in polyatomic molecules.

I. Introduction

The excited state dynamics of polyatomic molecules is dominated by the non-adiabatic coupling of vibrational and electronic degrees of freedom, inducing both charge and energy redistribution in molecules. These dynamics are the primary step in the photochemistry of many polyatomic molecules,¹ photobiological processes such as vision and photosynthesis² and underlie many concepts in molecular electronics.³ The Born–Oppenheimer (BO) approximation, an adiabatic separation of electronic and vibrational motions, is exact if the nuclear kinetic energy is negligible. Its breakdown is thus uniquely due to the motions of the atoms and occurs at the intersections or near intersections of potential energy surfaces belonging to different electronic configurations.^{4,5} The non-zero off-diagonal matrix elements of the nuclear kinetic energy operator couple the zeroth order electronic states, allowing us to define the so-called ‘promoting modes’. Stated differently, it is the ‘promoting modes’ which mix the initial ‘doorway’ BO state with a manifold of vibronic levels of a lower electronic state, leading to the radiationless ‘decay’ of the initial state. This ‘decay’ represents a conversion of electronic to vibrational energy and is thus often the first step in the ensuing photochemical dynamics. Non-adiabatic coupling^{6–10} often leads to complex, broadened absorption spectra due to the high density of nuclear states and strong variations of transition dipole with nuclear coordinate.

High resolution spectroscopy of small molecules provides the most detailed insights into non-adiabatic processes. In some larger molecules such as pyrazine, ‘exact’ solutions to the radiationless transition problem have been demonstrated.¹¹ In general, however, these problems

[†] Present address: LCAR, IRSAMC, Université Paul Sabatier, Toulouse, France.

[‡] Present address: Institut für Medizinische Optik, Ludwig-Maximilians-Universität, München, Germany.

[§] Present address: Institute of Physics and Astronomy, University of Aarhus, Århus, Denmark.

remain difficult, particularly when the state density becomes high and multi-mode vibronic couplings are involved. As a first step, characterizing the ‘reaction’ pathway by minimum energy path calculations¹² provides a picture of the mechanism. Full dimensional dynamical calculations of multi-mode vibronic coupling are yet to come. The case of greatest import to photochemistry—when the zeroth order excited states are directly or indirectly coupled to a true continuum, leading to non-adiabatic photodissociation dynamics^{13–15}—is especially challenging.

Rapid electronic dephasing leading to a strong reduction in transition dipole generally limits the spectroscopic ‘observation’ of excited state dynamics to times within the electronic dephasing time, T_2^* . A classic example of this is the $S_2 \leftarrow S_0$ absorption spectrum of butadiene in which the very broad vibrational structure cannot be resolved.¹⁶ Double resonance, such as resonance Raman spectroscopy, which projects the excited state back onto the ground electronic state, can reveal details of the *initial* excited state dynamics^{17–19} but, importantly, only for times on the order of T_2^* . In order to obtain information about the molecular dynamics after T_2^* , *i.e.* on the ‘dark’ state, double resonance techniques where the final state is *not* the ground electronic state will be useful.

In this Discussion, we wish to consider an alternative approach to these problems: the use of time domain methods.²⁰ The three aspects of a femtosecond pump–probe experiment are the preparation, the evolution and the probing of a non-stationary superposition state (a wavepacket). The amplitudes and initial phases of the prepared states are determined by the amplitude and phase distributions comprising the pump laser field and the transition probabilities involved. Once the pump laser pulse is over, the wavepacket $\chi(\Delta t)$, given by eqn. (1), evolves freely according to relative energy phase factors in the superposition.

$$|\chi(\Delta t)\rangle = \sum_n a_n |\Psi_n\rangle e^{-i2\pi c E_n \Delta t} \quad (1)$$

The a_n complex coefficients contain both the amplitudes and initial phases of the exact (non-BO) molecular eigenstates $|\Psi_n\rangle$ which are prepared by the pump laser. The E_n are the excited state eigenenergies, given here in wavenumbers. Although we show here only the case of discrete excited states, the description of a wavepacket can be readily extended to include continuous states.

The probe laser field interacts with the wavepacket after the pump pulse is over, by projecting it onto a specific final state $|\Psi_f\rangle$ at some time delay Δt . The time dependence of the signal, $S(\Delta t)$, can be thus visualized:

$$S(\Delta t) = |\langle \Psi_f | \vec{\mu} \cdot \vec{E} | \chi(\Delta t) \rangle|^2 = \left| \sum_n b_n e^{-2\pi c E_n \Delta t} \right|^2 \quad (2)$$

where

$$b_n = a_n \langle \Psi_f | \vec{\mu} \cdot \vec{E} | \Psi_n \rangle$$

$$S(\Delta t) = \sum_n \sum_{m \leq n} |b_n| |b_m| \cos\{(E_n - E_m)2\pi c \Delta t + \Phi_{nm}\}$$

The b_n complex coefficients contain the a_n from eqn. (1) as well as the probe transition dipole moment and generalized vibronic overlap factors to the final state. The measured signal $S(\Delta t)$ arises from a coherent sum over all two-photon transition amplitudes consistent with the pump and probe laser bandwidths involved and therefore implicitly contains interferences between degenerate two-photon transitions. It is the interference between individual two-photon transitions arising from an initial state, through *different* excited eigenstates and terminating in the *same* final state which leads to these modulations. The power spectrum of this time domain signal gives information about the set of level spacings in the problem and their respective overlaps with a specific, chosen final state.

The choice of the molecular ionization continuum as the final state $|\Psi_f\rangle$ in wavepacket experiments has several conceptual and practical advantages.²¹ (1) Charged particle detection is extremely sensitive. (2) Detection of the ion provides mass information. (3) Ionization is always an allowed process, with relaxed selection rules—any molecular state can be ionized (no ‘dark’ states). (4) Highly detailed, multiplexed information can be obtained by differentially analyzing the outgoing photoelectron as to its kinetic energy,^{22–30} angular distribution^{31–40} and spin polariza-

tion. (5) Higher order (multiphoton) processes, which can be difficult to avoid in femtosecond experiments, are readily revealed.

We wish to investigate the use of the molecular ionization continuum as a ‘template’ for the projection of complex non-adiabatic wavepacket dynamics. The ability to make differential measurements—*via* photoelectron spectroscopy—is a critical element of this scheme. Photoelectron spectroscopy is sensitive to both electronic configurations and vibrational dynamics.⁴¹ An elementary but useful picture is that emission of an independent outer valence electron occurs without simultaneous electronic reorganization of the ion core (the molecular orbital or Koopmans’ picture). These simple correlation rules indicate the cation state expected to be formed upon single photon, single active electron ionization of a given molecular orbital. Partial ionization probabilities into specific ion electronic states can differ drastically with respect to the molecular orbital nature of the neutral electronic state. If a given neutral electronic configuration correlates, upon removal of a single active outer valence electron, to the ground electronic configuration of the cation, then the photoionization probability is generally higher than if it does not.

In Fig. 1, we show a picture of excited state polyatomic wavepacket dynamics. A zeroth order bright state, α , is coherently prepared with a femtosecond pump pulse. According to the molecular orbital picture, it ionizes into the α^+ continuum, the electronic state of the ion obtained upon removal of the outermost valence electron. This process produces a photoelectron band ε_1 . In this example, we have chosen α^+ to be the ground electronic state of the ion. We now consider a non-adiabatic coupling process which transforms the zeroth order bright state α into a lower lying zeroth order dark state, β , as induced by promoting vibrational modes of the appropriate symmetry. By the same arguments, the β state should ionize into the β^+ ionization continuum, producing a photoelectron band ε_2 . Here we assume that β^+ is an electronically excited state of the cation. Therefore, if we use a sufficiently energetic probe photon such that both the α^+ and β^+ continua are open channels, we expect a *switching* of the electronic photoionization channel from ε_1 to ε_2 during the non-adiabatic process. This simple picture suggests that one might be able to monitor directly the evolving excited state electronic configurations (*i.e.* the electronic *population* dynamics) during non-adiabatic processes while simultaneously following the coupled nuclear dynamics *via* the vibrational structure within each photoelectron band. A simple relevant question in intramolecular dynamics is: how can we experimentally distinguish the effects of IVR (that is the mixing of zeroth order vibrational functions by intermode coupling) which occurs on a single potential surface, from non-adiabatic dynamics which leads to a mixing of electronic states and subsequently induces IVR? In the manner discussed above, we could distinguish IVR from non-

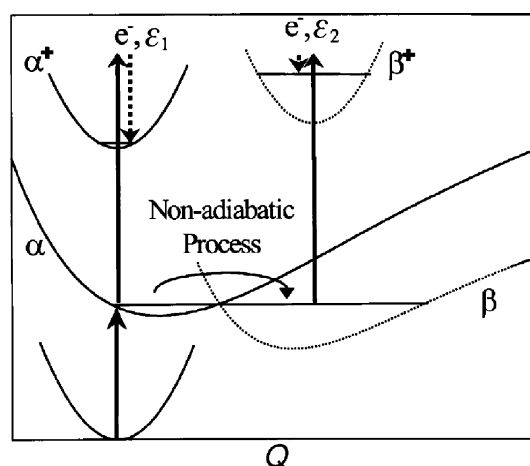


Fig. 1 A picture of polyatomic non-adiabatic dynamics. The α state prepared by the pump laser decays into the lower lying β state due to non-adiabatic coupling. Here we assume that for these two states the Koopmans'-type correlations upon ionization are complementary: the α state ionizes into the α^+ ground state ion continuum whereas the β state ionizes into the β^+ ion continuum. This scheme should allow the disentangling of electronic from vibrational dynamics during non-adiabatic processes, as discussed in the text.

adiabatic dynamics because only the latter can cause a switching of the continuum electronic channels. This ‘disentangling’ of electronic from vibrational dynamics during non-adiabatic processes could give a new, detailed view of excited polyatomic molecules.³⁰ We assume for the moment that two-hole one-particle excitations, which can spoil the molecular orbital picture for *inner* valence photoionization, will generally appear at higher photon energies than we are concerned with here ($\epsilon_{\text{tot}} < 15\text{--}20$ eV).^{42,43} We also initially neglect autoionizing resonances which potentially interfere with the simple molecular orbital picture,⁴⁴ due to the broad bandwidths involved in femtosecond measurements (typically 30–60 meV), the effect of any single resonance is diluted.

We discuss two limiting cases for Koopmans’-type correlations in such experiments. The first case is when the neutral excited states α and β clearly correlate to *different* ion electronic continua, as suggested by Fig. 1. Even if there are large geometry changes upon internal conversion and/or ionization, producing long vibrational progressions, such strong electronic correlations should favour a disentangling of the vibrational dynamics from the electronic population dynamics, as discussed above. Case (1) systems are found, for example, in the photodynamics of linear polyenes and, below, we discuss the specific example of all-*trans* decatetraene. The other limiting case is when the neutral excited states α and β correlate equally strongly to the *same* ion electronic continua. This is expected to hinder the disentangling of electronic from vibrational dynamics. Case (2) systems are found, for example, in the photodynamics of polyaromatic hydrocarbons and, below, we discuss the specific example of phenanthrene. We note, however, that the increased vibrational energy is still expected to affect the form of the photoelectron spectra even in case (2) systems. The ability to distinguish the vibrational dynamics in the α and β states will depend therefore on the molecule-specific geometry changes between these neutral states and the ion state.

In other cases, neither the Koopmans’-type correlations nor the geometry changes upon ionization might favour the disentangling of vibronic dynamics. Nevertheless, time-resolved photoelectron spectroscopy might still be useful for following non-adiabatic dynamics if one is able to resolve the photoelectron emission angle. Unless the promoting mode is totally symmetric, the electronic symmetries of the coupled BO states will differ. This symmetry difference translates, upon ionization, into a change of the photoelectron angular distribution (PAD) during the course of the non-adiabatic process. The PADs are sensitive to both the nuclear rotational motion and the symmetry of the electronic wavefunction.³³ In a later section, we discuss this approach and the opportunities it may present for experiment.

We have thus far discussed the non-adiabatic dynamics of bound excited states. The case of excited states coupled to a dissociative continuum represents the important problem of non-adiabatic photodissociation dynamics. In such cases, it becomes very difficult to follow complex excited state dynamics as it proceeds towards dissociation. Hope remains in looking at the product elimination channels in more detail. Examples include the time evolution of the product translational energy and internal energy distributions. The time evolution of various vector correlations and alignments are other differential measures of product attributes which could be considered. Time resolved photoelectron spectroscopy can also be applied as a differential probe to these problems, as discussed in a concluding section of this paper.

II. Experimental

Amplified, independently tunable (207–300 nm) femtosecond pump and probe laser pulses (60–150 fs, 0.1–5 μJ) were brought collinearly and co-propagating into the interaction region of a molecular beam photoelectron spectrometer. Both a linear time-of-flight and a magnetic bottle spectrometer were employed. Both spectrometers were also used to record mass spectra. Variable temperature pulsed and continuous nozzles were used to control the molecular beam composition. Temporal and spatial overlap of the laser pulses as well as the photoelectron energy calibration was obtained using nitric oxide and xenon gas. The pulse energies were adjusted so that one photon processes dominated for the pump and probe steps. The experiments consisted of recording photoelectron spectra at a series of time delays between the pump and probe laser pulses. The photoelectron spectra had the signals of one laser subtracted. Experimental details are reported elsewhere.^{21,45}

III. Case (1), complementary Koopmans'-type correlations: linear polyenes

In order to give an example of case (1) type correlations, we consider ultrafast internal conversion in the linear polyene all-*trans* 2,4,6,8-decatetraene (DT).⁴⁶ The first optically allowed transition is $(S_2)1^1B_u \leftarrow (S_0)1^1A_g$. The S_2 state is a singly excited configuration. The lowest excited state is the dipole forbidden $(S_1)2^1A_g$ state⁴⁷ which arises from configuration interaction between singly and doubly excited A_g configurations. Non-adiabatic coupling, leading to ultrafast internal conversion from S_2 to S_1 is prompted by b_u symmetry vibrational motions. The molecular orbitals which play an important role in the internal conversion of DT can be seen in Table 1. These calculated excited electronic states of the molecule and cation radical were obtained with the QCFF/PI + CISD method.^{48,49} The ionization energies of the continua discussed here are low enough that two-hole one-particle excitations are unattainable and Koopmans' approximation applies.⁵⁰ The right-hand column of Table 1 shows the electronic configuration of the ion which correlates with the neutral excited state upon removal of the outermost electron. It can be seen that the S_0 ground state and the S_2 excited state both correlate with the $(D_0)1^2B_g$ ground electronic state of the cation. The S_1 state, by contrast, correlates predominately with the $(D_1)1^2A_u$ first excited state of the cation.

In Fig. 2(a) we show the energy level scheme relevant to this experiment. A femtosecond pump pulse at 287 nm (4.32 eV) prepared the excited S_2 state at its vibrationless electronic origin. It then evolves into a vibrationally hot (0.7 eV) S_1 electronic state *via* internal conversion. The idea is to observe the rapidly evolving electronic states by projecting the wavepacket onto several cation electronic states using a UV probe photon of sufficient energy (here, 235 nm, 5.27 eV). As the non-adiabatic coupling proceeds, the evolving electronic character of the wavepacket alters the photoionization electronic channel, leading to large shifts in the time-resolved photoelectron spectrum.³⁰

The experimental photoelectron kinetic energy spectra in Fig. 2(b) are characterized by a rapid shift of electrons from an energetic component ($\epsilon_1 = 2.5$ eV) to a broad, structured low energy component (ϵ_2). The pump and probe laser polarizations were parallel to the electron spectrometer axis. This shift is the *direct* (as opposed to inferred) signature of the changing electronic state induced by non-adiabatic coupling. The 2.5 eV band is due to ionization of the S_2 into the D_0 ion state. The broad, low energy band arises from photoionization of S_1 which correlates with the D_1 ion state. Its appearance is due to population of the S_1 state by internal conversion. Integration of the two photoelectron bands directly reveals the S_2 to S_1 internal conversion time scale of 386 ± 65 fs. It is important to note that these results contain much more information than the overall (integrated) internal conversion time. The vibrational structure in each photoelectron band

Table 1 Calculated molecular orbitals and configuration interaction in a case (1) molecule, all-*trans* decatetraene^a

Electronic state	Energy/eV	Molecular orbital occupancy						Weight	Correlated ion state
		1a _u	1b _g	2a _u	2b _g	3a _u	3b _g		
Neutral									
$S_0, 1^1A_g$	0	2	2	2	2			100%	1^2B_g
$S_1, 2^1A_g$	3.6	2	2	2	0	2		33%	1^2A_u
		2	2	1	2	1		33%	1^2A_u
		2	2	2	1	0	1	33%	1^2B_g
$S_2, 1^1B_u$	4.3	2	2	2	1	1		100%	1^2B_g
Cation									
$D_0, 1^2B_g$	IP = 7.3	2	2	2	1			97%	
$D_1, 1^2A_u$	8.5	2	2	1	2			50%	
		2	2	2	0	1		50%	

^a The state of the cation expected upon the single photon, single active electron (Koopmans') photoionization of each state is given in the right hand column. It can be seen that the correlations upon ionization for the S_2 and S_1 states are (mostly) complementary.

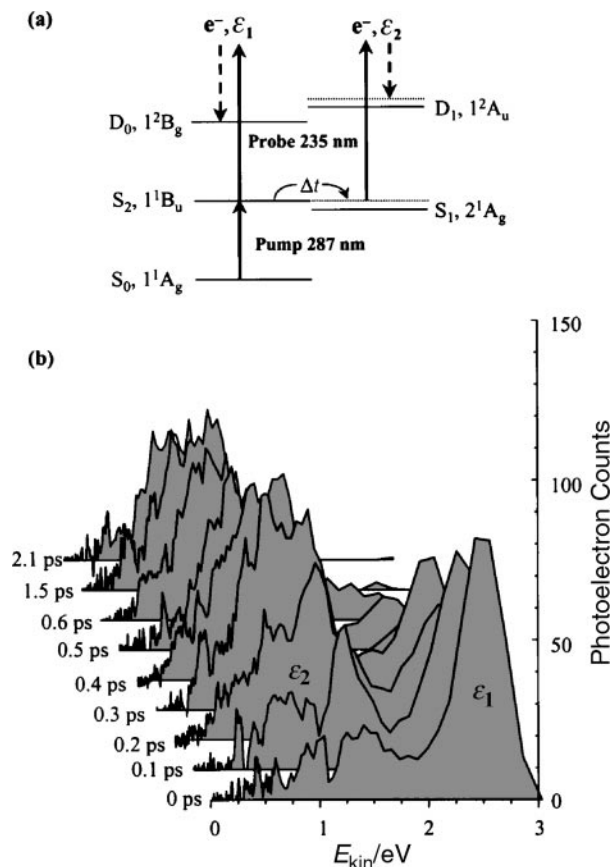


Fig. 2 Time-resolved vibrational and electronic dynamics during internal conversion for a case (1) molecule, all-*trans* decatetraene (DT). (a) Level scheme in DT for one-photon probe ionization. The pump laser prepares the optically bright state S_2 . Due to ultrafast internal conversion, this state converts to the lower lying state S_1 with 0.7 eV of vibrational energy. The expected ionization propensity rules are shown: $S_2 \rightarrow D_0 + e^-(\epsilon_1)$ and $S_1 \rightarrow D_1 + e^-(\epsilon_2)$. (b) Femtosecond time-resolved photoelectron kinetic energy spectra of DT pumped at 287 nm and probed at 235 nm. There is a rapid shift (≈ 400 fs) in the distribution: from (ϵ_1) an energetic peak at 2.5 eV due to photoionization of S_2 into the D_0 cation ground electronic state, to (ϵ_2) a broad, structured band at lower energies due to photoionization of vibrationally hot S_1 into the D_1 cation first excited electronic state. These results show a disentangling of electronic population dynamics from vibrational dynamics. The structure in the low energy band reflects the vibrational dynamics in S_1 .

yields information about the state-to-state vibrational dynamics which promote and tune the electronic population transfer, as well as the evolution of the ensuing IVR in the “hot molecule” which occurs on the S_1 potential surface. These above results have been completely confirmed by independent measurements using two-photon ionization of the coupled S_2 – S_1 states.³⁰ Multi-mode quantum dynamical simulations, in progress, are expected to shed light on these vibrational dynamics.

This case (1) example of decatetraene demonstrates the selectivity of the molecular ionization continuum for specific neutral configurations. Furthermore, it shows that for favourable Koopmans'-type correlations, the electronic population dynamics can indeed be disentangled from the vibrational dynamics. This promises to yield detailed new views of multi-mode non-adiabatic coupling in polyatomic systems and permit direct observation of the evolution of IVR and the onset of statisticality on the potential surface populated by the process (*i.e.* the ‘dark’ state).

IV. Case (2), similar Koopmans'-type correlations: polyaromatic hydrocarbons

We now consider case (2) systems in which the one-electron correlations upon ionization lead to the same cationic states. In this case we would not expect such a favourable separation of electronic from vibrational dynamics, as was seen for the case (1) example of DT. Examples of case (2) systems include the polyaromatic hydrocarbons and here we consider the specific example of S_2 - S_1 internal conversion in phenanthrene (PH). In Table 2 the molecular orbital configurations and their approximate weights are shown for the electronic states of PH, obtained with the QCFF/CISD method. The ground S_0 state is a single configuration while the S_1 and the S_2 states consist of two configurations with a 1 : 1 and 3 : 1 weight respectively. The result of Koopmans' approximation is shown in the last column of Table 2. It can be seen that in the case of PH both the S_2 and S_1 states correlate similarly with the electronic ground state as well as with the first excited state of the cation. This should be contrasted with the complementary correlations of DT in Table 1.

As illustrated in Fig. 3(a), we excited PH from the S_0 1A_1 ground state to the origin of the S_2 1B_2 state with a 282 nm (4.37 eV) fs pump pulse. The excited molecules are then ionized after a time delay Δt using a 207.5 nm (5.98 eV) probe photon. The S_2 1B_2 state rapidly internally converts to the lower lying S_1 1A_1 state at 3.63 eV, transforming electronic into vibrational energy. The Koopmans'-type correlations expected for single photon, single active electron ionization, as given in Table 2, are shown by the downwards arrows. It can be seen that both the S_2 1B_2 and S_1 1A_1 states can correlate with the D_0 2B_1 ion ground state, producing the ε_1 and ε_4 photoelectron bands. They can also each correlate with the D_1 2A_1 ion excited state, producing the electron bands ε_2 and ε_5 .

In Fig. 3(b) we show molecular beam magnetic bottle (angle integrated) photoelectron spectra for PH as a function of time delay between pump and probe pulses.⁴⁵ The pump and the probe laser polarization were parallel to the electron TOF axis. The photoelectron spectra reveal a rapidly decaying but energetically narrow peak at $\varepsilon_1 \approx 2.5$ eV. This peak is due to photoionization of the vibrationless S_2 1B_2 state into the ionic ground state D_0 2B_1 , as expected based on Table 2. In order to monitor the zeroth order S_2 electronic population decay, this time dependent peak was integrated and plotted as a function of time, resulting in a decay time constant of 522 ± 16 fs. This confirms a previous 0.5 ps result based upon rotational deconvolution of the S_2 absorption lineshape.⁵¹ The broad band, centered at about 1.5 eV, in these photoelectron spectra is partly due to ionization of vibrationally hot molecules in the S_1 state formed by the internal conversion but also contains other components, as discussed in the following. Normally one would expect this 1.5 eV

Table 2 Calculated molecular orbitals and configuration interaction in a case (2) molecule, phenanthrene^a

Electronic state	Energy/eV	Molecular orbital occupancy						Weight	Correlated ion state
		a ₂	a ₂	b ₁	a ₂	b ₁	b ₁		
Neutral									
S_0 , 1A_1	0	2	2	2				100%	2B_1
S_1 , 1A_1	3.6	2	2	1	0	1		50%	2B_1
		2	1	2	1			50%	2A_2
S_2 , 1B_2	4.4	2	2	1	1			75%	$2B_1$
		2	1	2	0	1		25%	$2A_2$
Cation									
D_0 , $2B_1$	IP = 7.9	2	2	1				100%	
D_1 , $2A_2$	8.4	2	1	2				100%	
D_2 , $2A_2$	9.3	1	2	2				100%	

^a The state of the cation expected upon the single photon, single active electron (Koopmans') photoionization of each state is given in the right hand column. It can be seen that the correlations upon ionization for the S_2 and S_1 states are the same.

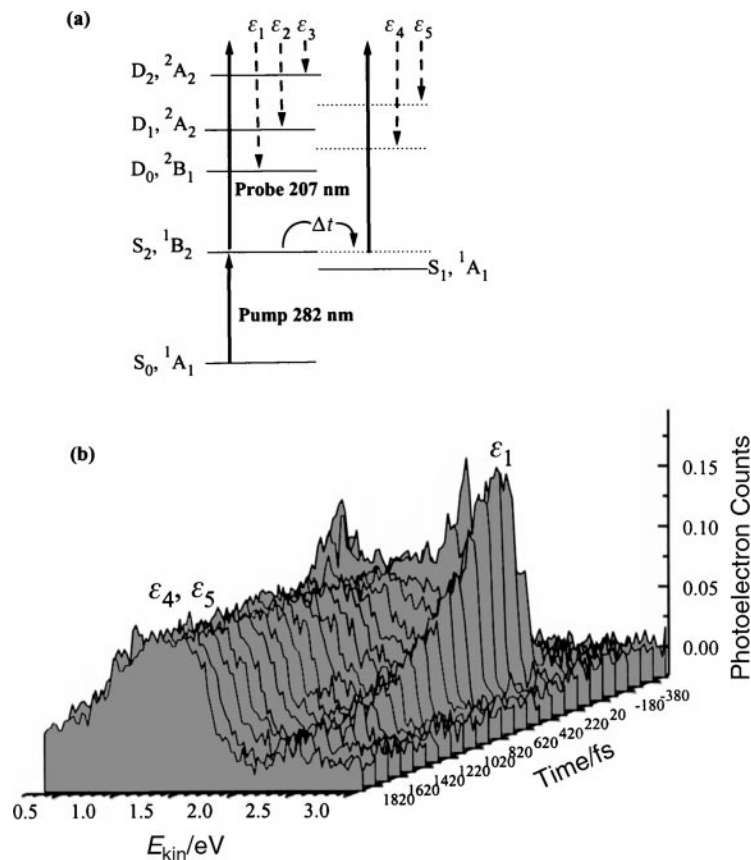


Fig. 3 Time-resolved vibrational and electronic dynamics during internal conversion for a case (2) molecule, phenanthrene (PH). (a) Level scheme in PH for one-photon probe ionization. The pump laser prepares the optically bright state S_2 . Due to ultrafast internal conversion, this state converts to the lower lying state S_1 with 0.74 eV of vibrational energy. The expected ionization propensity rules are shown: $S_2 \rightarrow D_0, D_1, D_2 + e^-$ ($\epsilon_1, \epsilon_2, \epsilon_3$) and $S_1 \rightarrow D_0, D_1 + e^-$ (ϵ_4, ϵ_5). (b) Femtosecond time-resolved magnetic bottle photoelectron kinetic energy spectra of PH pumped at 282 nm and probed at 207 nm. There is a rapid shift (≈ 500 fs) in the distribution: from (ϵ_1) an energetic peak at 2.5 eV due to photoionization of S_2 into the D_0 cation ground electronic state; to a broad, structured band at lower energies (0.5–1.5 eV). Due to the high probe photon energy, at short times this band contains both decaying (ϵ_2, ϵ_3) and growing (ϵ_4, ϵ_5) components. At longer times (> 500 fs), the signal is due to photoionization of vibrationally hot S_1 into the D_0 (ϵ_4) and D_1 (ϵ_5) vibrationally excited cation states. The structure in the low energy band also reflects the vibrational dynamics in S_1 .

band to grow as a function of time due to population flow into the S_1 state, as in the case of DT internal conversion. This simple picture is not observed in this measurement because the probe laser photons had sufficient energy (5.98 eV) to project the intermediate state non-adiabatic wavepacket produced by the pump laser onto several cation electronic states. Fig. 3(a) shows that up to four photoionization bands (ϵ_2 – ϵ_5) can in principle contribute to this 1.5 eV feature, although ionization out of the S_2 state into the second excited ionic state D_1 (ϵ_3) should be less favourable because of the Koopmans' propensity rules (see Table 2). The broad component of the photoelectron spectra we observed around 1.5 eV is therefore, at short times, a superposition of both decaying (ϵ_2, ϵ_3) and growing (ϵ_4, ϵ_5) photoelectron bands. Generally one can expect that the photoelectron bands arising from ionization out of the S_1 state should be broader than those arising from the electronic origin of the S_2 state because of the ongoing IVR in the vibrationally hot molecule on the S_1 potential energy surface. At times $t > 1500$ fs or so (*i.e.* after internal

conversion), the 1.5 eV band is comprised almost exclusively of signals due to S_1 ionization (ϵ_4 and ϵ_5). As can be seen, the S_1 state itself is long lived on the time scale of our experiment.

Despite the fact that case (2) molecules present an unfavourable case for disentangling electronic from vibrational dynamics, we can still see for the case of PH a dramatic shift in the photoelectron spectrum as a function of time. This is due to the fact that PH is a rigid molecule and the S_2 , S_1 and D_0 states all have similar geometries. The photoionization probabilities are therefore expected to be dominated by small Δv transitions. Hence, the 0.74 eV vibrational energy in the populated S_1 state should be roughly conserved upon ionization into the D_0 ionic state. That is to say, we would expect the edge of the ϵ_4 band to be shifted to lower energies by about 0.74 eV as compared with the ϵ_1 band. Indeed this is what is observed in Fig. 3(b). Therefore, for PH, small geometry changes favour conservation of vibrational energy upon ionization and thereby permit the observation of the excited state electronic population dynamics *via* a photoelectron kinetic energy analysis alone. A similar situation was noted for the case of DABCO (triethylenediamine).⁵² More generally, larger geometry changes upon internal conversion and ionization would mean that bands such as ϵ_1 and ϵ_4 would overlap, as in the case of S_1 to S_0 internal conversion in hexatriene.²⁵ In such cases, a clear disentangling of electronic from vibrational dynamics using the kinetic energy distribution alone is more challenging. In the next section we discuss an alternate route towards the disentangling of electronic from vibrational dynamics in excited molecules.

V. Photoelectron angular distributions

Time-resolved photoelectron angular distributions (PADs) were shown to be sensitive probes of nuclear hyperfine coupling in NO,³² field-induced alignment,³⁴ and rotation–vibration coupling mechanisms.^{35,38,40} In these studies, the PADs evolve due to the changes in the rotational dynamics of the wavepacket. PADs are also revealing of detailed vibrational wavepacket dynamics.³⁷ It has been pointed out^{33,30} and recently shown³⁹ that PADs provide a potentially useful probe of electronically non-adiabatic polyatomic dynamic. In this case, the change in angular distribution reflects the time evolution of the zeroth order electronic composition of the wavepacket.

In non-adiabatic transitions, the zeroth order electronic symmetry of the BO states changes in the course of the process if the promoting mode is non-totally symmetric. Since the product of the symmetry species of the neutral electronic state, the dipole operator, the ion electronic state and the free electron wavefunction must be invariant under all symmetry operations of the molecular point group, a symmetry difference between the coupled electronic states translates into a change of the symmetry of the outgoing electron waves. Similar consideration apply for the case of inter-system crossing.³⁹

In the energy domain, PADs have been shown to provide an extremely sensitive probe of the ionization dynamics—sufficiently sensitive to extract the ionization bound–free amplitudes from rotationally resolved measurements.⁵³ Femtosecond experiments, particularly in larger systems, sum over all rovibrational states of the ion, integrate over the range of electron energies spanned by the pulses and average over a Boltzmann distribution of initial rotational levels. All Franck–Condon allowed angular momentum states of the departing electron can contribute and the selectivity of the energy domain measurements with respect to l is lost. The important characteristic that survives this averaging is the electronic symmetry.³⁹ As a consequence of the extensive averaging, the sensitivity of the PAD to radial contributions to the electron–core scattering is reduced, rendering it a potentially useful probe of wavepacket motions rather than being obscured by details of photoionization dynamics. From the theoretical view point, this suggests approximate models that take the electronic and rotational symmetries and the angular momentum algebra into extract account while simplifying the details of the electron–core interaction. Ref. 39 generalizes the previously developed non-perturbative theory³³ for calculation of PADs from linear systems to arbitrary molecules and re-expresses the observables in a way that exposes and utilizes the electronic and the rotational symmetries. The formally exact (non-perturbative in the field) expression for the time-resolved PAD of an arbitrary molecule is given³⁹ as the squared modulus of the time-dependent amplitude of a state-resolved continuum eigenstate, integrated over the range of photoelectron energies spanned by the probe bandwidth. A sequence of approx-

imations is then introduced, systematically reducing the formally exact expressions to simpler forms that could be applied to more complex systems.

In general, a non-perturbative treatment of the field is important since it is in practice difficult to perform amplified femtosecond laser experiments which are in the Golden rule (perturbative) limit (*e.g.* $< 10^8 \text{ W cm}^{-2}$). This is a simple consequence of the energy of the pulse being delivered in a very short time. For example, a $1 \mu\text{J}$ pulse at 330 nm under even moderate focussing conditions ($f/40$) achieves an intensity of $10^{12} \text{ W cm}^{-2}$. The effects of non-perturbative fields depend on the observable. The probe laser intensity has only a minor effect on the form of the PAD in the intensity range of interest considered here.³⁴ The pump field, by contrast, has a significant effect which is particularly pronounced in PADs due to the phenomenon of rotational excitation and alignment in moderately intense near-resonant laser fields.⁵⁴ While strong fields may complicate the interpretation of the observable if not properly accounted for, the intensity property of short pulse can also serve to advantage. In order to avoid rotational excitation, the pump duration should be small compared to the relevant Rabi period, $\tau < \Omega_R^{-1}$. It should be pointed out, however, that this can lead to unacceptably small pump–probe signals. In order to gain physical insight, it is instructive to introduce Golden rule approximations for the pump and probe steps, providing expressions that expose the temporal and angular dependence of the signal and allow analytical solutions for part of the problem. This is discussed in the paragraph below. [We note that for angle integrated electron *energy* distribution measurements, the intensity effects are much less apparent. The effects of alignment (due to the pump laser) are insignificant and the ponderomotive broadening of the photoelectron spectrum (due to the probe laser) is typically smaller than the effective laser bandwidths.⁵⁵]

Averaging over the parent and ion magnetic states reduces the PAD to the form³⁹

$$\sigma(\Delta t, \hat{k}) = \frac{\sigma_{\text{tot}}(\Delta t)}{4\pi} [1 + \beta_2(\Delta t)P_2(\cos \theta_k) + \beta_4(\Delta t)P_4(\cos \theta_k)] \quad (3)$$

where $\hat{k} = (\theta_k, \phi_k)$ denotes the scattering direction of the photoelectron with respect to the space-fixed frame. Eqn. (3) applies to the case of common linear polarization of the pump and probe electric fields. With other polarization arrangements the cylindrical symmetry is broken and $\sigma(\Delta t, \hat{k})$ acquires a ϕ_k -dependence, providing complementary views of the wavepacket symmetry. The form of the total cross section $\sigma_{\text{tot}}(\Delta t)$ and the asymmetry parameters $\beta_i(\Delta t)$, which contain the full wavepacket dynamics, are given explicitly in ref. 39. We note here only that $\sigma_{\text{tot}}(\Delta t)$ oscillates on the vibrational time-scales while the asymmetry parameters respond to the rotations (and rotation–vibration coupling) and specifically carry the information about the electronic character of the wavepacket that evolves with time in the course of a non-adiabatic transition.

In order to expose the information content of the time-resolved PAD it is helpful initially to introduce further approximations. If attention is confined to time-delays shorter than rotational coherence times, it is possible to separate the rotational and vibronic motions and sum analytically over the rotational states. In this limit the PAD can be cast in the form³⁹

$$\sigma(\Delta t, \hat{k}) = \sum_{\nu_1 \nu_1'} G_{\nu_1 \nu_1'}(\Delta t) \times \sum_{\eta \zeta} F_{\nu_1 \nu_1' \eta \zeta} \times g_{\eta \zeta}(\hat{k}) \quad (4)$$

where the ν_i are vibrational indices in the excited state, η denotes collectively the excitation and ionization photon indices and ζ includes all indices required to specify the electronic states. The G contain the details of the pump and probe pulses and the time delay between them. The g are analytic functions that can be thought of pictorially as transforming the symmetry of the electronic wavefunctions with respect to the body-fixed frame into anisotropy of the space-fixed angular distribution. The F contain the details of the vibronic Hamiltonian, the bound–bound wavepacket preparation amplitudes and the bound–free electronic ionization amplitudes. The F functions couple the time evolution contained in G with the scattering angle dependences in g and thus give rise to the change of the asymmetry parameters with time in the course of a non-adiabatic transition.

Qualitative insight into the type and magnitude of such a change can be gained by computing the cross section at two time instances, corresponding to ionization from either of the BO states. For this purpose, it is sufficient to compute the electronic bound–free amplitudes (the matrix elements of the dipole operator between the bound and free electronic states) for each of the BO

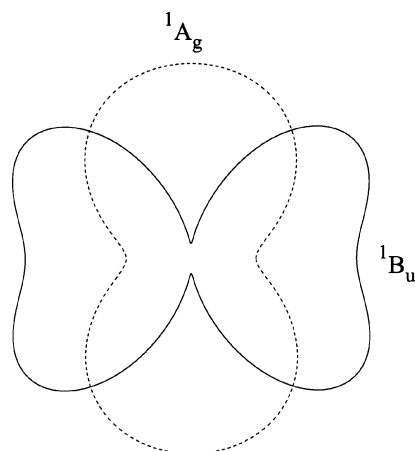


Fig. 4 Calculated lab frame PADs, using the methods described in ref. 39, for the zeroth order (S_2) 1^1B_u and (S_1) 2^1A_g states of octatetraene (OT). It can be seen that the difference in electronic symmetry leads to very different lab frame PADs for these two states, suggesting that such changes should be experimentally observable.

states, bypassing for now the calculation of the vibronic Hamiltonian and the multidimensional wavepacket motion on the coupled electronic states.

Accurate calculation of these electronic amplitudes for polyatomic systems of chemical interest is not practical. As discussed above, however, the nature of femtosecond-resolved experiments in large systems, along with the dominant character of the effect, suggest simple approximations. Provided that the electronic and rotational symmetries are taken into exact account in the g of eqn. (4) and in the angular part of the electronic amplitudes, the radial part of the electron core scattering dynamics (the numerically costly part of the calculation) can be crudely approximated.

Here, we expand the free electron states in generalized harmonics^{56,57} appropriate to the C_{2h} point group and approximate the radial coefficients by Coulomb waves. Specifically we examine, as an experimentally relevant example, the PADs for ionization from the bright and dark states of octatetraene (OT) which undergoes similar dynamics to that of DT, discussed above. Since our description of the bound and free electronic states is approximate, the results should be considered as pertaining to a general model with the symmetry properties of the *trans*-polyene family.

Requiring the product of irreducible representation of the bound and free electronic orbitals and the dipole operator to be invariant under the symmetry operations of the C_{2h} point group, we find that ionization of the S_2 state produces free electron wavefunctions of b_g symmetry for transitions polarized parallel to the molecular plane and of a_g symmetry for transitions polarized perpendicular to the plane. Ionization of the S_1 state, by contrast, results in scattering wavefunctions of a_u symmetry for plane-polarized transitions and of b_u symmetry for transitions polarized perpendicular to the molecular plane. For centrosymmetric systems, this division of the continuum into free electron states of even and odd parity is expected.⁵⁸

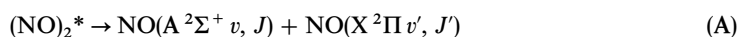
In Fig. 4, we show the lab frame PADs, calculated under the approximations discussed above, for ionization of the (S_2) 1^1B_u and (S_1) 2^1A_g states of OT into the ground (D_0) 1^2B_g state of the cation. It can be seen that there are significant differences in the PADs, suggesting that a time-resolved experiment might successfully follow this internal conversion.

VI. Non-adiabatic photodissociation dynamics

The most interesting case for photochemistry is that of unbound excited states or excited states coupled to a dissociative continuum. Many photoinduced polyatomic unimolecular reactions are based upon ‘hot molecules’ formed *via* ultrafast internal conversion.⁵⁹ A fundamental question in unimolecular reaction rate theory is that of the assumption of statistical energy redistribution due to IVR being very fast compared with reaction.⁶⁰ Many models and interpretations are based

upon the supposition of fast, complete IVR. Increasingly, however, this assumption has come into question since preparation of an excited molecule with a photon is very specific, quite unlike preparation by collision. There is a need for new experimental measures of the extent and time scale of vibrational energy redistribution in an isolated, energized molecule. Unimolecular decay theories make predictions about the time-distribution function for appearance of the products (*e.g.* exponential *vs.* power law). These theories do not make any predictions about more detailed product attributes, such as energy distributions. Therefore, energy resolved measurements of product state distributions, which are determined by exit valley forces, cannot yield information about the statisticality of the reaction. Time resolved photoelectron spectroscopy might allow us to measure the *time evolution* of the product attributes such as internal state and translational energy distributions or the angular momentum polarization and thereby provide new tests of the statistical assumption, beyond the rate constant.

As a simple example of the use of time-resolved photoelectron spectroscopy in non-adiabatic effects photodissociation dynamics, we consider the case of the *cis*-planar nitric oxide dimer.²⁹ The UV absorption spectrum is broad and featureless⁶¹ spanning the range 190–240 nm with a maximum at 205 nm, suggestive of a direct dissociation process. Studies of the photodissociation dynamics at 193 nm revealed that two product channels are open:⁶²



At 193 nm, the energies available to channels (A) and (B) are 0.93 eV and 0.69 eV, respectively. The observed NO(A,B) product state distributions were quite broad. Subsequent studies on the alignment and vector correlations⁶³ of the excited state products showed only quite weak effects, perhaps somewhat in contradiction with a direct dissociation mechanism.

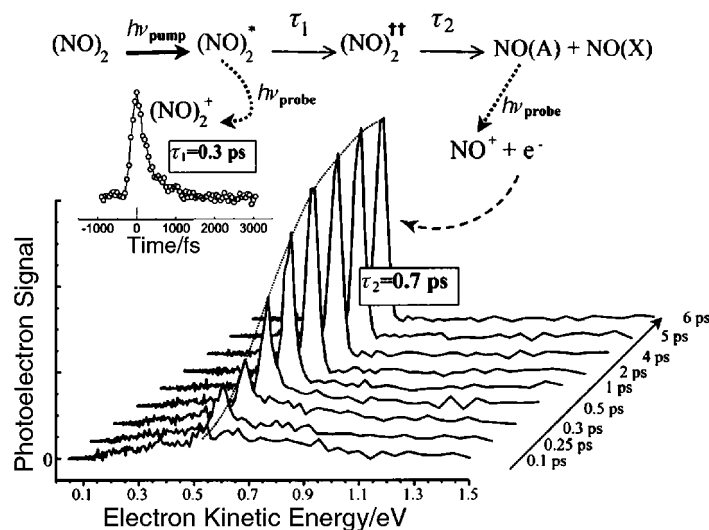


Fig. 5 Non-adiabatic photodissociation dynamics of the NO dimer. The pump laser excited the molecule to an excited state $(\text{NO})_2^*$. The probe laser ionizes this state after a time delay, producing $(\text{NO})_2^+$. The excited state molecule eventually dissociates, producing $\text{NO}(\text{A}) + \text{NO}(\text{X})$. The $\text{NO}(\text{A})$ product can be single photon ionized by the same probe laser, producing a sharp electron peak. Analysis of these results suggests a two-step non-adiabatic dissociation process. (Inset) The total parent ion $(\text{NO})_2^+$ signal plotted as a function of time delay. A simple fit yields a time constant of 0.3 ps, perhaps suggesting a direct dissociation. (Main) Time-resolved photoelectron spectra, showing a growing sharp feature at 0.52 eV due to appearance of the $\text{NO}(\text{A})$ product. Plotting the integral of this peak as a function of time yields a time constant of 0.7 ps, significantly slower than the decay of the parent ion signal. These results suggest that there is an intermediate state $(\text{NO})_2^{\ddagger\dagger}$, formed by non-adiabatic coupling from $(\text{NO})_2^*$ on a time scale τ_1 , and it is $(\text{NO})_2^{\ddagger\dagger}$ which decays to products on a longer time scale, giving an overall decay time τ_2 . These results illustrate the utility of differential (*e.g.* photoelectron) probes in non-adiabatic dissociation dynamics.

Broad featureless absorption spectra can also arise from ultrafast non-adiabatic processes in the excited state whose time scale may be unrelated to the dissociation time scale. In a time-resolved photoelectron spectroscopy experiment, it should be possible to distinguish a *direct* from a *step-wise non-adiabatic* photodissociation process *via* consideration of the effect of an evolving electronic symmetry on the photoionization dynamics.

In Fig. 5 (inset), we show a pump–probe signal of the decaying $(\text{NO})_2^+$ parent ion signal as a function of the time delay. The pump and probe wavelengths were 210 and 287 nm, respectively. A single exponential fit to the decay yields a time constant of 322 ± 12 fs. This could be interpreted (incorrectly) as the dissociation time of the excited state. In Fig. 5, we show femtosecond pump–probe photoelectron spectra for a series of time delays. The prominent feature is a sharp peak at 0.52 eV which grows with time, on a broad background which disappears with time. The sharp peak is the well known $\Delta v = 0$ $\text{NO}(\text{A } ^2\Sigma^+, v) \rightarrow \text{NO}^+(\text{X } ^1\Sigma^+, v)$ ionizing transition.⁶⁴ Neither the ground state $\text{NO}(\text{X } ^2\Pi)$ nor the excited state $\text{NO}(\text{B } ^2\Pi)$ product are ionized at 287 nm: the former because of its high ionization potential, the latter, because of its unfavourable electronic configuration for single photon, single active electron ionization. The appearance time of the $\text{NO}(\text{A})$ state product, the 0.52 eV electron peak, is considerably slower (0.7 ps) than the disappearance time of the parent ion signal (0.3 ps). The difference in time scales between parent ion signal disappearance and product signal appearance suggests a two-step non-adiabatic mechanism. The non-adiabatic decay of the $(\text{NO})_2^*$ state on a time scale $\tau_1 \approx 0.3$ ps, is to another excited state $(\text{NO})_2^{\dagger\dagger}$ which has a relatively poor ionization cross section, presumably due to an unfavourable electronic configuration. This suggests why the parent ion signal decays in 0.3 ps even though the molecule has not dissociated. It is this second (“dark”) state which decays to the products on a longer time scale, giving an overall decay time of $\tau_2 \approx 0.7$ ps. These results show how the time-resolved integrated parent ion signal alone can be misleading in polyatomic dynamics, due to changes in electronic symmetry, and that differential methods such as photoelectron spectroscopy can help to elucidate the dynamics. The possibility to extract even more information about non-adiabatic dissociation dynamics using femtosecond time-resolved coincidence techniques such as angle-resolved photoelectron–photoion coincidence (ARPEPICO) is discussed below.

VII. Conclusions and future directions

The non-adiabatic dynamics of polyatomic molecules is an important yet difficult problem in photochemistry. The multi-dimensional mixing of vibrational with electronic degrees of freedom, leading to high level densities and strongly varying transition moments, presents a challenge to high resolution spectroscopy. A complementary approach is *via* the use of time domain (femtosecond pump–probe) methods. In these techniques, the choice of final state—the template for wavepacket projection—is of critical importance. We have argued that the molecular ionization continuum should be an interesting final state for non-adiabatic polyatomic wavepackets. The vibrational aspects of the wavepacket dynamics can be observed *via* the vibrational structure of the ionization continuum (*i.e.* vibrational states of the cation). The electronic structure of the continuum (*i.e.* the set of electronic states of the cation and the free electron partial wave structure) is sensitive to the electronic population dynamics (based on electronic propensity rules and symmetry properties of the free electron waves). In order to develop a more general basis for this technique, two questions require further attention. (1) To what extent does the breakdown of the molecular orbital picture play a role in the outer valence shell photoionization dynamics of polyatomic molecules? (2) To what extent may the effects of sharp autoionizing resonances affect the global picture of the photoionization dynamics viewed by broad band pulses?

In our ongoing experimental work, we are applying time-resolved magnetic bottle photoelectron spectroscopy to a variety of problems. An example of chemical interest is excited state proton transfer in *o*-hydroxybenzaldehyde (salicylaldehyde), yielding both time scales and the energy dependences of the intramolecular processes.⁶⁵ In the area of molecular electronics, azobenzene serves as a model ultrafast molecular switch. We have studied the non-adiabatic intramolecular dynamics of azobenzene, determining time scales and shedding new light on the primary photo-physical processes.⁶⁶ Of photochemical interest, the excited states of aldehydes and ketones, by contrast with polyenes, have important carbonyl π – π^* and n – π^* interactions. In order to make comparisons, we have examined the non-adiabatic dynamics in a series of molecules containing

two double-bonds: butadiene, propenal, methyl vinyl ketone and acryloyl chloride.⁶⁷ These above results will be discussed in forthcoming publications. In the future, we plan to investigate excited state electron transfer dynamics using time-resolved photoelectron spectroscopy, with the hope of directly observing the coherent vibrational dynamics associated with the charge transfer.⁶⁸

In our ongoing theoretical work, we have developed a numerically efficient multi-mode quantum dynamical model of vibronic coupling and are applying it to the simulation of time-resolved photoelectron spectra of wavepacket dynamics in linear polyenes.⁶⁹ We hope that these results will allow the extraction of the detailed vibrational dynamics from data of the type shown in Fig. 2. Future work will further explore the possibility of using angle-resolved photoelectrons in the dynamics of non-adiabatic processes. The application of the formalism of ref. 39 to a variety of systems of different symmetries would be necessary in order to establish the generality of the method, its range of applicability and its limitations. While such exploration is best carried out within the crudest of the hierarchy of approximations introduced in ref. 39, it will be important to refine the model by systematically removing one or more of the approximations involved, as appropriate for the application sought. The development or adaptation of improved methods for computing electronic scattering wavefunctions that remain applicable to chemically interesting systems would permit quantitative calculation of the PAD at fixed delay times. More interesting would be the application of the full formalism³⁹ to compute the PAD as a function of the time delay, taking into account the vibronic dynamics. An exciting opportunity is that of exploiting the intensity property of short-pulse lasers to enhance the utility of the method for probing the underlying electronic symmetry. This will be explored by removing the Golden rule approximation to treat the field non-perturbatively.

By introducing increasingly differential measures it is possible to develop time- and mass-resolved photoelectron probes. A first step in this direction, using PEPICO detection, was shown for the study of mass resolved intracuster dynamics.⁷⁰ We plan to use time-resolved PEPICO to investigate the role of solvent effects in excited state proton and electron transfer *via* the use of mass resolved clusters. These same methods should be applicable to photodissociation dynamics. Even more details are obtained from correlating the photofragment recoil momentum vector with the coincident photoelectron momentum vector. The ARPEPICO method can yield molecular frame PADs for axially recoiling dissociative ion states⁷¹ and dissociative photodetachment of molecular anions.⁷² Recently, a time-resolved ARPEPICO method was demonstrated for the study of NO₂ multiphoton dissociation dynamics, correlating the NO(A) photofragment energy-angle resolved recoil with photoelectron energy-angle resolved emission.⁷³ In polyatomic dissociation dynamics, such correlations could shed light on quite complex processes. As an example, in the case of the NO dimer discussed above, a femtosecond pump-probe ARPEPICO technique could yield NO(A) photofragment recoil frame PADs and their variation with recoil energy. This could provide a view of the photofragment angular momentum polarization and *v*-*J* correlations as a function of time during “statistical” unimolecular decay. In the energy domain, atomic angular momentum polarization measurements have shown sensitivity to details of the photodissociation dynamics.⁷⁴ Time domain measurements could give a new perspective on the approach to statistical behaviour in unimolecular decay. Uncorrelated signals such as the lab frame angle-resolved photofragment kinetic energy release as a function of time could yield information about the rate of phase space sampling during unimolecular decay.⁷⁵ An ARPEPICO apparatus based upon a pair of high resolution timing-imaging (crossed delay line anode) MCP detectors is presently under construction in our laboratory.⁷⁶ These opportunities will be explored in our future experimental and theoretical research.

Acknowledgements

S. Lochbrunner and M. Schmitt thank the Deutsche Forschungsgemeinschaft for financial support. J. J. Larsen thanks the Danish government for financial support.

References

- 1 J. Michl and V. Bonacic-Koutecky, *Electronic Aspects of Organic Photochemistry*, Wiley, New York, 1990.
- 2 R. W. Schoenlein, L. A. Peteanu, R. A. Mathies and C. V. Shank, *Science*, 1991, **254**, 412.
- 3 J. Jortner and M. A. Ratner, *Molecular Electronics*, IUPAC, Blackwell, Oxford, 1997.

- 4 G. Herzberg and H. C. Longuet-Higgins, *Faraday Discuss.*, 1963, **35**, 77.
- 5 The spin-orbit operator is also sometimes called a non-adiabatic operator. The BO states, however, can be defined as states of impure spin multiplicity which are unmixed by spin-orbit coupling. The nuclear kinetic energy operator has a unique role.
- 6 M. Bixon and J. Jortner, *J. Phys. Chem.*, 1968, **48**, 715.
- 7 J. Jortner, S. A. Rice and R. M. Hochstrasser, *Adv. Photochem.*, 1969, **7**, 149.
- 8 B. R. Henry and W. Siebrand, in *Radiationless Transitions in Organic Molecular Photophysics*, ed. J. B. Birks, Wiley, London, 1973, vol. I, p. 152.
- 9 K. F. Freed, in *Radiationless Processes in Molecules and Condensed Phases*, ed. F. K. Fong, Springer, Berlin, 1976, p. 23.
- 10 G. Stock and W. Domcke, *Adv. Chem. Phys.*, 1997, **100**, 1.
- 11 J. Kommandeur, W. M. Majewski, W. L. Meerts and D. W. Pratt, *Ann. Rev. Phys. Chem.*, 1987, **38**, 433.
- 12 M. Garavelli, F. Bernardi, M. Olivucci, T. Vreven, S. Klein, P. Celani and M. A. Robb, *Faraday Discuss.*, 1998, **110**, 51.
- 13 For example, A. D. Bandrauk and M. S. Child, *Mol. Phys.*, 1970, **19**, 95; M. S. Child and R. B. Bernstein, *J. Chem. Phys.*, 1973, **53**, 5916; M. S. Child, *Mol. Phys.*, 1976, **32**, 1495.
- 14 R. Schinke, *Photodissociation Dynamics*, Cambridge University Press, Cambridge, 1993.
- 15 L. J. Butler, *Ann. Rev. Phys. Chem.*, 1998, **49**, 125.
- 16 G. Orlandi, F. Zerbetto and M. Z. Zgierski, *Chem. Rev.*, 1991, **91**, 867.
- 17 W. Siebrand and M. Z. Zgierski, *J. Chem. Phys.*, 1979, **71**, 3561.
- 18 R. J. Sension, R. J. Boudryushi, B. S. Hudson, F. Zerbetto and M. Z. Zgierski, *J. Chem. Phys.*, 1992, **96**, 2617.
- 19 M. K. Lawless, S. D. Wickam and R. A. Mathies, *Acc. Chem. Res.*, 1995, **28**, 493.
- 20 A. H. Zewail, *Femtochemistry*, World Scientific, Singapore, 1994.
- 21 (a) I. Fischer, D. M. Villeneuve, M. J. J. Vrakking and A. Stolow, *J. Chem. Phys.*, 1995, **102**, 5566; (b) I. Fischer, M. J. J. Vrakking, D. M. Villeneuve and A. Stolow, *Chem. Phys.*, 1996, **207**, 331.
- 22 M. Seel and W. Domcke, *J. Chem. Phys.*, 1991, **95**, 7806.
- 23 V. Engel, *Chem. Phys. Lett.*, 1991, **178**, 130; Ch. Meier and V. Engel, *Chem. Phys. Lett.*, 1993, **212**, 691; Ch. Meier and V. Engel, *J. Chem. Phys.*, 1994, **101**, 2673; Ch. Meier and V. Engel, *Phys. Rev. Lett.*, 1994, **73**, 3207.
- 24 B. Kim, C. P. Schick and P. M. Weber, *J. Chem. Phys.*, 1995, **103**, 6903.
- 25 D. R. Cyr and C. C. Hayden, *J. Chem. Phys.*, 1996, **104**, 771.
- 26 A. Assion, M. Gelsler, J. Helbing, V. Seyfried and T. Baumert, *Phys. Rev. A*, 1996, **54**, R4605.
- 27 B. J. Greenblatt, M. T. Zanni and D. M. Neumark, *Chem. Phys. Lett.*, 1996, **258**, 523.
- 28 W. Radloff, V. Sert, Th. Freudenberg, I. V. Hertel, C. Juvet, D. Dedonder-Lardeux and D. Solgadi, *Chem. Phys. Lett.*, 1997, **281**, 20.
- 29 V. Blanchet and A. Stolow, *J. Chem. Phys.*, 1998, **108**, 4361.
- 30 V. Blanchet, M. Z. Zgierski, T. Seideman and A. Stolow, *Nature*, 1999, **401**, 52.
- 31 K. L. Reid, *Chem. Phys. Lett.*, 1993, **215**, 25.
- 32 K. L. Reid, S. P. Duxon and M. Towrie, *Chem. Phys. Lett.*, 1994, **228**, 351.
- 33 T. Seideman, *J. Chem. Phys.*, 1997, **107**, 7859.
- 34 S. C. Althorpe and T. Seideman, *J. Chem. Phys.*, 1999, **110**, 147.
- 35 K. L. Reid, T. A. Field, M. Towrie and P. Matousek, *J. Chem. Phys.*, 1999, **111**, 1438.
- 36 T. Suzuki, L. Wang and H. Kohguchi, *J. Chem. Phys.*, 1999, **111**, 4859.
- 37 Y. Arasaki, K. Takatsuka, K. Wang and V. McKoy, *Chem. Phys. Lett.*, 1999, **302**, 363.
- 38 S. C. Althorpe and T. Seideman, *J. Chem. Phys.*, submitted.
- 39 T. Seideman, *J. Chem. Phys.*, submitted.
- 40 T. Seideman and S. C. Althorpe, *J. Electron Spectrosc. Relat. Phenom.*, in press.
- 41 J. H. D. Eland, *Photoelectron Spectroscopy*, Butterworths, London, 1984.
- 42 L. S. Cederbaum, W. Domcke, J. Schirmer and W. von Niessen, *Adv. Chem. Phys.*, 1986, **65**, 115.
- 43 For example, P. Baltzer, L. Karlsson, B. Wannberg, G. Öhrwall, D. M. P. Holland, M. A. MacDonald, M. A. Hayes and W. von Niesser, *Chem. Phys.*, 1997, **224**, 95.
- 44 For example, D. M. P. Holland, M. A. MacDonald, M. A. Hayes, L. Karlsson and B. Wannberg, *J. Electron Spectrosc. Relat. Phenom.*, 1999, **104**, 245.
- 45 S. Lochbrunner, J. J. Larsen, T. P. Shafter, M. Schmitt, T. Schultz, J. G. Underwood and A. Stolow, *J. Electron Spectrosc. Relat. Phenom.*, submitted; M. Schmitt, J. J. Larsen, S. Lochbrunner, J. P. Shafter, M. Z. Zgierski and A. Stolow, *J. Chem. Phys.*, submitted.
- 46 H. Petek, A. J. Bell, K. Yoshihara and R. L. Christensen, *J. Chem. Phys.*, 1991, **95**, 4739.
- 47 J. R. Andrews and B. S. Hudson, *Chem. Phys. Lett.*, 1978, **57**, 600.
- 48 A. Warshel and M. Karplus, *J. Am. Chem. Soc.*, 1972, **94**, 5612.
- 49 F. Zerbetto, M. Z. Zgierski, F. Negri and G. Orlandi, *J. Chem. Phys.*, 1988, **89**, 3681.
- 50 G. Fronzoni, G. P. Declava, A. Lisini and G. De Alti, *J. Electron Spectrosc. Relat. Phenom.*, 1994, **69**, 207.
- 51 A. Amirav, M. Sonnenschein and J. Jortner, *J. Phys. Chem.*, 1984, **88**, 5593.
- 52 C. C. Hayden, personal communication.

- 53 For example, H. Park and R. N. Zare, *J. Chem. Phys.*, 1996, **104**, 4554; H. Park and R. N. Zare, *J. Chem. Phys.*, 1996, **104**, 4568.
- 54 T. Seideman, *J. Chem. Phys.*, 1995, **103**, 7887.
- 55 A. Zavriyev, I. Fischer, D. M. Villeneuve and A. Stolow, *Chem. Phys. Lett.*, 1995, **234**, 281.
- 56 P. G. Burke, N. Chandra and F. A. Gianturco, *J. Phys. B: At. Mol. Phys.*, 1972, **5**, 2212.
- 57 N. Chandra, *J. Phys. B: At. Mol. Phys.*, 1987, **20**, 3405; N. Chandra, *J. Phys. B: At. Mol. Phys.*, 1987, **20**, 3417.
- 58 D. Dill and U. Fano, *Phys. Rev. Lett.*, 1972, **29**, 1203.
- 59 W. Wild, A. Seilmeier, N. H. Gottfried and W. Kaiser, *Chem. Phys. Lett.*, 1985, **119**, 259.
- 60 W. Forst, *Theory of Unimolecular Reactions*, Academic Press, New York, 1973.
- 61 J. Billingsley and A. B. Callear, *Trans. Faraday Soc.*, 1971, **67**, 589.
- 62 O. Kajimoto, K. Honma and T. Kobayashi, *J. Phys. Chem.*, 1985, **89**, 2725.
- 63 Y. Naitoh, Y. Fujimura, K. Honma and O. Kajimoto, *J. Phys. Chem.*, 1995, **99**, 13652.
- 64 J. C. Miller and R. N. Compton, *J. Chem. Phys.*, 1981, **75**, 22.
- 65 S. Lochbrunner, A. Stolow *et al.*, manuscript in preparation.
- 66 T. Schultz, A. Stolow *et al.*, manuscript in preparation.
- 67 J. P. Shaffer, A. Stolow *et al.*, manuscript in preparation.
- 68 M. Bixon and J. Jortner, *J. Chem. Phys.*, 1997, **107**, 1470.
- 69 S. Alavi, T. Seideman *et al.*, work in progress.
- 70 V. Stert, W. Radloff, C. P. Schultz and I. V. Hertel, *Eur. Phys. J. D*, 1999, **5**, 97.
- 71 P. Downie and I. Powis, *Phys. Rev. Lett.*, 1999, **82**, 2864.
- 72 K. A. Hanold, M. C. Garner and R. E. Continetti, *Phys. Rev. Lett.*, 1996, **77**, 3335.
- 73 J. A. Davies, J. E. LeClair, R. E. Continetti and C. C. Hayden, *J. Chem. Phys.*, 1999, **111**, 1.
- 74 For example, Z. H. Kim, A. J. Alexander and R. N. Zare, *J. Phys. Chem., A*, 1999, **103**, 10144.
- 75 J. P. Shaffer and A. Stolow, work in progress.
- 76 J. P. Shaffer, C. C. Hayden and A. Stolow, work in progress.